Intraoral radiography using dual imaging plates with 12-block horizontal enlargement correction

Takahito Sekiguchi

Nihon University Graduate School of Dentistry,

Major in Oral and Maxillofacial Radiology

(Directors: Prof. Yoshinori Arai and Assoc. Prof. Kunihito Matsumoto)

Contents

This thesis is based on the article listed below with additional data.

Sekiguchi T, Kato M, Kimoto H, Amemiya T, Dezawa K, Imanishi Y, Matsumoto K, Arai Y (2023) Correction of intraoral radiography with dual imaging plates using enlargement of the horizontal direction with division into 12 blocks. J Oral Sci 65, 40-43.

Summary

Intraoral radiography with imaging plates (IPs) was established in the 1990s and has been used worldwide. IPs consist of a support layer, a photostimulable phosphor (PSP) layer, and other layers. The PSP absorbs X-ray energy after irradiation with X-rays and emits light photons with an intensity corresponding to the amount of absorbed X-ray energy when irradiated with an appropriate wavelength laser (red scan beam) in a scanner. The photomultiplier tube in the scanner detects the light photons and the electronic signal produced by analog-to-digital conversion is then converted to a digital image. The scanned IPs are reusable after erasure of image information in PSP layer by emission of intense visible light. The IP itself can be reused 200-1,000 times or more. During operations of intraoral radiography such as insertion of the IP into the oral cavity and encapsulation, artifact of the IP system is distortion of images caused by curving of the IP and malfunction of the reader during IP scanning.

The dual imaging plate (DIP) method, which synthesizes intraoral radiographs from a front imaging plate (FIP) and a back imaging plate (BIP), produces adequate image quality and allows the radiation dose to be reduced. In the DIP method, it is necessary to precisely match the FIP and BIP images using the least squares method. In other words, the subtraction image of the FIP and BIP is synthesized, and the standard deviation (SD) is calculated. The synthesis is repeated while shifting the BIP image little by little so that the SD reaches the minima value. At the position where the SD reaches the minima value, the synthesis image is performed to obtain the DIP image. Positional misalignment and differences in distortion between the FIP and BIP images influence accuracy in synthesizing DIP images. No studies have examined in detail the correction method and the value of shifting the BIP image. Therefore, this study aimed to establish positional correction in the DIP method by correcting the enlargement ratio in the horizontal direction and the effect of the method of dividing the IP area into 12 blocks to correct the enlargement ratio. Additionally, the effect and imaging processing time of the correction

method are also evaluated.

Six sets of two imaging plates (12 IPs) were used for imaging a mesh plate and a porcine mandible phantom. Asahi X-ray Xspot-TS was used as the X-ray generator. The imaging conditions were tube voltage 60 kV, tube current 6 mA and exposure time 0.1 s. The focus to DIP distance was set at 40 cm. After irradiation, the FIP and BIP images were read using Digora Optime and output in 8-bit gray-scale BMP format. Further image processing was performed with the original software developed by Visual Studio 2019 C#. The details of the method of aligning the two images are set out below:

1) The simple subtraction image and the synthesized DIP image were combined without shifting the position of the FIP and BIP images.
2) The BIP was moved in vertical and horizontal directions so that the SD of the subtraction image became the minima.
3) The BIP was rotated so that the SD of the subtraction image became the minima.
4) The enlargement ratio of the BIP was changed in the horizontal direction so that the SD of the subtraction image became the minima. The maximum and minimum of the enlargement ratio of each DIP were calculated.
5) Finally, the area of the horizontal direction of the IP was divided into 12 blocks. The enlargement ratio in the horizontal direction was changed at each area so that the SD of the subtraction image became the minima.

The *F*-value was calculated to compare variance of the pixel values on the subtraction images between each step. When the *F*-value was higher than the *F* critical value (1.00183), it was interpreted as a statistically significant difference in variance of the pixel values in the subtraction images between the two steps ($P < 0.01$). The image processing times for steps 1–4 and 1–5 were also compared for six sets of DIPs imaged for each phantom three times.

In the mesh plate phantom, the minimum and maximum of the horizontal enlargement ratio were 1.006 and 1.032, respectively. The minimum of the horizontal

enlargement ratio of each block of each set was 0.975, and the maximum was 1.008 when divided into 12 blocks. The SD was significantly degraded by additional processing in all sets. The SD was significantly reduced by the addition of the correction of enlargement in the horizontal direction and the correction of the horizontal direction when divided into 12 blocks. Statistical analysis showed a significant reduction in the variance of the pixel value with the additional process ($P < 0.01$). In the porcine mandible phantom, statistical analysis also revealed a significant reduction in the variance of the pixel value with the additional process ($P < 0.01$). Means of the image processing times for mesh plate phantom were 10.82 s (SD, 0.64) for steps 1–4 and 15.96 s (SD, 1.27) for steps 1–5. Means of the image processing times for porcine mandible phantom were 11.27 s (SD, 0.57) and 18.22 s (SD, 1.46) for steps 1–4 and steps 1–5, respectively. There was a statistically significant extension of the imaging processing time when the IP area was divided into 12 blocks to correct the enlargement ratio in both comparisons ($P < 0.05$).

In the DIP method, the variance and SD of the subtraction image from the FIP and BIP were significantly reduced by correcting the horizontal, vertical, rotational, and enlargement ratio in the horizontal direction. Furthermore, by dividing the IP into 12 blocks in the horizontal direction and adjusting the enlargement ratio of each block in the horizontal direction, the SD of the subtraction image was reduced. The enlargement ratio was changeable among the 12 blocks in an IP, indicating inconstant IP movement speed along the long axis during scanning. Additional correction by dividing the IP area horizontally into 212 blocks made it possible to synthesize more precise DIP images. The extended image processing time by adding this correction was less than 10 s and may be acceptable for clinical use.

Introduction

Intraoral radiography with imaging plates (IPs) was established in the 1990s and has been used worldwide [1-6]. IPs consist of a support layer, a photostimulable phosphor (PSP) layer, and other layers. The PSP absorbs X-ray energy after irradiation with X-rays and emits light photons with an intensity corresponding to the amount of absorbed X-ray energy when irradiated with an appropriate wavelength laser (red scan beam) in a scanner. The photomultiplier tube in the scanner detects the light photons and the electronic signal produced by analog-to-digital conversion is then converted to a digital image [7]. The scanned IPs are reusable after erasure of image information in PSP layer by emission of intense visible light.

The IP itself can be reused 200-1,000 times or more [8-10]. During intraoral radiography, operations such as insertion of the IP into the oral cavity, encapsulation and removal of the plastic cover to prevent saliva and infection, and reading by a laser scan often result in adhesion of adhesive from the plastic covers and scratches on the IP surface [5]. This causes artifacts on the intraoral radiographs [11,12]. Another artifact of the IP system is distortion of images caused by curving of the IP and malfunction of the reader during IP scanning [13].

Watanabe et al. [14] described the principles of the dual imaging plate (DIP) method, which uses two IPs, a front IP (FIP) and a back IP (BIP), for taking intraoral radiographs. The DIP method produces a synthesized image with the two images from the FIP and BIP. The authors concluded that the DIP method can produce an intraoral radiograph with adequate image quality and a reduced radiation dose. Imanishi et al. [15] reported that artifacts caused by dirt and scratches can be corrected when using the DIP method in combination with image subtraction. In the DIP method, it is necessary to precisely match the FIP and BIP images using the least squares method. In other words, the subtraction image of the FIP and BIP is synthesized, and the standard deviation (SD) is calculated. The synthesis is repeated while shifting the BIP image little by little so that

the SD reaches the minima value. At the position where the SD reaches the minima value, the synthesis image is performed to obtain the DIP image. Positional misalignment and differences in distortion between the FIP and BIP images influence accuracy in synthesizing DIP images.

No studies have examined in detail the correction method and the value of shifting the BIP image. Therefore, this study provides a detailed analysis of the positional correction method in the DIP method. Additionally, the effect of correcting the enlargement ratio in the horizontal direction, the effect of the method of dividing the IP area into 12 blocks to correct the enlargement ratio and the imaging processing time are also evaluated.

Materials and Methods

DIP preparation

Six sets of DIPs (12 IPs; Digora Optime Imaging Plate size 2, PaloDEx Group Oy, Tuusula, Finland) were used in the study. Following the method of Watanabe et al. [14], the thin iron plate of the FIP was first peeled off. The FIP and BIP were stacked and placed in a plastic bag (disposable cover for the Digora Optime imaging plate, size 2, Tanaka-ya Co., Tokyo, Japan).

Phantoms and imaging

Two phantoms were used: a 1-mm mesh plate (Dentech Corp. Tokyo, Japan) and a porcine mandible embedded in acrylic resin. For imaging of the mesh plate, the phantom was closely adhered to the front surface of the plastic bags. For imaging of the porcine mandible, the phantom was set according to the parallel method [16].

Asahi X-ray Xspot-TS (Asahi Roentgen Ind., Co., Kyoto, Japan) was used as the X-ray generator. The imaging conditions were tube voltage 60 kV, tube current 6 mA and

exposure time 0.1 s. The focus to DIP distance was set at 40 cm in accordance with previous studies [14,15].

Image processing

After irradiation, the FIP and BIP images were read using Digora Optime DXR-60 (PaloDEx Group Oy). The pixel size for the reading was 30 μm × 30 μm and the number of pixels was 1,200 × 1,000. The images were output in 8-bit gray-scale BMP format.

Further image processing was performed with the original software developed by Visual Studio 2019 C # (Microsoft Corp., Redmond, WA, USA). The details of the method of aligning the two images are set out below:

1) The simple subtraction image and the synthesized DIP image were combined without shifting the position of the FIP and BIP images. The value of the shift vector was displayed as a two-dimensional image. In this image, each position on the IP is displayed every 50 pixels vertically and horizontally. The value of the shift vector is indicated by the direction of the shift and the length of shift. The length of the vector is twice the actual length of displacement.
2) The BIP was moved in vertical and horizontal directions so that the SD of the subtraction image became the minima. The results are shown in the shift vector images, subtraction images, and synthesized DIP images.
3) The BIP was rotated so that the SD of the subtraction image became the minima.
4) The enlargement ratio of the BIP was changed in the horizontal direction so that the SD of the subtraction image became the minima, as shown in Fig. 1a. The maximum and minimum of the enlargement ratio of each DIP were calculated.
5) Finally, the area of the horizontal direction of the IP was divided into 12 blocks as shown in Fig. 1b, and the enlargement ratio in the horizontal direction was changed at each area so that the SD of the subtraction image became the minima. The shift vector image, the subtraction image, and the synthesized image of each DIP were

also obtained. The maximum and minimum of the enlargement ratio of each block in each set were calculated.

The image processing times of steps 1–4 and 1–5 were also measured for six sets of DIPs imaged for each phantom three times.

Statistical processing

The variance and SD of the pixel value in the subtraction image were obtained for each step from the first to the fifth correction after verification of the normality of the pixel value in the subtraction image using the frequency distribution tables. The sample number for calculation of the variance and SD was 1,080,000 pixels (1,200 × 900) at the center of the IP. The total number of pixels used for the statistical analysis was 6,480,000 in six IPs. The *F*-value was calculated to compare variance of the pixel values on the subtraction images between each step as follows:

F-value = s_1^2 / s_2^2

s^2: variance of pixel value, $[s_1^2 > s_2^2]$

The *F* Distribution Calculator [17] was used to calculate the *F* critical value of which the rejection area (α) and degree of freedom were set as 0.01 and 6,479,999, respectively. Finally, when the *F*-value was higher than the *F* critical value, it was interpreted as a statistically significant difference in variance of the pixel values in the subtraction images between the two steps ($P < 0.01$).

The mean time for imaging processing per set of three DIP measurements was used for statistical analysis. The image processing times between steps 1–4 and 1–5 were compared using the paired *t*-test after verification of the normal distribution of measurements using the Shapiro-Wilk test. Statistical analysis of the image processing times was performed using SPSS Version 25.0 (IBM Corp., Armonk, NY, USA). A *P*-value of less than 0.05 was considered statistically significant.

Results

Mesh plate phantom

Six sets of DIP images were obtained. One example of FIP and BIP images is shown in Fig. 2. Figure 3-1 shows an image obtained in the first step as a simple subtraction without shifting the position. Each position of the shift vector image (a) is shown with small points, so the length of the vector is zero with no direction of the vectors. The subtraction image (b) is depicted by black and white mesh lines. The DIP image shows a section with double lines due to misalignment of the FIP and BIP (Fig. 3-1c; black arrowhead). Figure 3-2 shows an image in which the shift in the horizontal and vertical directions is corrected. The shift vector extended uniformly in the lower direction. Although the white arrowhead in Fig. 3-2c indicates a section where the FIP and BIP were matched, the other sections (black arrowhead) are out of alignment. Figure 3-3 shows images after rotational movement. The shift vector shows zero length near the central left of the IP. The length of the vector increases in proportion to the distance from the central rotational point, and the direction of the vector spread concentrically. Although the section indicated by the white arrowhead was matched, the lower right edge of the IP appears as a double line (black arrowhead), demonstrating the result of correcting the enlargement in the horizontal direction. The shift vector changed slightly compared with that of Fig. 3-3a. Although the subtraction image was greatly improved, the section indicated by the dotted arrowhead was slightly mismatched (Fig. 3-4c). Figure 3-5 shows the results of correction by dividing the IP area into 12 blocks. The white arrowhead also indicates the section that is better matched than that of Fig. 3-4c.

The minimum and maximum of the horizontal enlargement ratio were 1.006 and 1.032, respectively. The minimum of the horizontal enlargement ratio of each block of each set was 0.975, and the maximum was 1.008 when divided into 12 blocks.

Figure 4 shows changes in the absolute value of the SD of the pixel value in the six sets of subtraction images at each of the five processes. The SD was significantly

degraded by additional processing in all sets. Additionally, the SD was significantly reduced by the addition of the correction of enlargement in the horizontal direction and the correction of the horizontal direction when divided into 12 blocks. Statistical analysis showed a significant reduction in the variance of the pixel value with the additional process ($P < 0.01$; Table 1).

The mean of the image processing time for mesh plate phantom was 10.82 s (SD, 0.64) for steps 1–4 and 15.96 s (SD, 1.27) for steps 1–5 (Fig. 5), indicating a statistically significant extension of the imaging processing time by adding the correction step (dividing the IP area into 12 blocks to correct the enlargement ratio) ($P < 0.05$).

Porcine mandible phantom

FIP and BIP images of the porcine mandible are shown in Fig. 6. Figure 7-1 is a simple subtraction image. The first row (a), second row (b), and third row (c) are shift vector images, subtraction images, and DIP images, respectively. The black circles in Fig. 7 indicate double lines, which improved step by step from 1) to 5), as indicated by white circles. SDs decreased from 9.20 to 6.93. Finally, the double line at the upper left of the image in Fig. 7-5b disappeared. Statistical analysis revealed a significant reduction in the variance of the pixel value with the additional process ($P < 0.01$; Table 2).

The mean of the image processing time for porcine mandible phantom was 11.27 s (SD, 0.57) for steps 1–4 and 18.22 s (SD, 1.46) for steps 1–5 (Fig. 5), indicating a statistically significant extension of the imaging processing time by adding the correction step (dividing the IP area into 12 blocks to correct the enlargement ratio) ($P < 0.05$). The extended image processing time was 6.96 s (95% confidence interval, 5.72–8.20).

Discussion

Watanabe et al. [14] reported that the contrast-to-noise ratio increased and the noise decreased in DIP images in which FIP and BIP were synthesized in intraoral radiography. Another problem with IP is that scratches and dust cause artifacts. This issue was addressed by Imanishi et al. [15], who reported that DIP with image processing could reduce artifacts. In DIP, the FIP and BIP images are shifted by the least squares method until the SD of the different images becomes the minima. The sensitivity of FIP and BIP may differ. Therefore, sensitivity correction is required. In this study, the mean densities of the two Ips were matched by correcting for differences in sensitivity. First, the processing obtained the SI of FIP image and BIP image. If there is a perfect match, the SI will be noise only and the pixel SD of SI will be the minimum. If the images do not match, the SI will show an embossed image and the SD will be large. The BIP image is shifted so that this SD is minimized. The trajectory becomes a vector image.

In the least squares method, the position of the BIP image is moved slightly and the calculation is repeated so that the SD of SI is minimized. The main movement methods are X and Y directions and rotation. The location of the minimum value of SD can be obtained by moving 1 pixel equivalent. The operation ends when the minimum of the SD is obtained. However, the method and value of this shift have not been reported or examined in detail. Therefore, in this experiment, the status of the fitting was confirmed at each step using a 1-mm mesh plate phantom.

If FIP and BIP are read in exactly the same positional relationship, the images match perfectly, and the SD of the subtraction image between the two images also takes a minimum value. However, in reality, the IP was slightly shifted to the left or right, up or down, or with a slight rotation (Fig. 3-1). Then, in the first step, the BIP was shifted in a horizontal and vertical direction to reduce the SD (Fig. 3-2). However, due to deviation or distortion, double lines were observed at the edges of the subtraction image and the DIP image. The second step added rotational correction, and the double lines were

diminished (Fig. 3-3).

If the only cause of image distortion was a shift to the left or right, up or down, or rotation, the double lines should disappear with the shifting at this point. However, as shown by the black arrowhead in Fig. 3-3c, the double lines were still observed. This was due to an error in the horizontal enlargement ratio between the FIP and BIP.

The IP moves in the reading device in the direction of the long axis of the IP (that is, in the horizontal, right, or left direction on the image). When the red laser beam scans along the short axis of the IP, if there is a latent image of the X-rays in the IP, that part emits blue light and is imaged [5,6]. Currently, if the movement speed of the Ips in the direction of the long axis was slightly different between the FIP and BIP, the horizontal enlargement ratios of the two images would be slightly different on the image. If they matched perfectly, the enlargement ratio would be 1.000, and there would be no change. In this experiment, when the horizontal enlargement ratio was corrected and the least squares method was used, the enlargement ratio was 1.032 at the maximum. This indicates that the rate was caused by an error in the movement of the IP in the direction of the long axis during scanning. Most images were converged by the correction of the enlargement ratio in the direction of the long axis (Fig. 3-4). However, even after this correction, a dull vertical line was observed at the right end of the IP (dotted line arrowhead, Fig. 3-4c). Therefore, the IP was divided into 12 blocks in the horizontal direction (Fig.1-b), and the magnification was corrected independently for each block. The maximum and minimum values of magnification were 1.008 and 0.975, respectively. As a result, the vertical line (white arrowhead, Fig. 3-5c) at the right end of the IP was almost erased, and the FIP and BIP images could be almost completely matched. Figures 7-5b and 7-5c were better matched than Fig. 7-4. This showed that the IP movement speed in the direction of the long axis at the time of reading was not completely constant. If the IP movement speed could be performed at a completely constant speed, the correction into 12 blocks and correction in the horizontal direction would be unnecessary to match the FIP and BIP

images of the DIP.

The image processing time was significantly extended by adding the correction of dividing the IP area horizontally into 12 blocks. The extension of the image processing time by adding this correction in the porcine mandible phantom, which simulated clinical conditions, was less than 10 s and may be substantially acceptable for clinical use. In the DIP method, the variance and SD of the subtraction image from the FIP and BIP were significantly reduced by correcting the horizontal, vertical, rotational, and enlargement ratio in the horizontal direction. Furthermore, by dividing the IP into 12 blocks in the horizontal direction and adjusting the enlargement ratio of each block in the horizontal direction, the SD of the subtraction image was reduced. This made it possible to synthesize more precise DIP images.

Conclusions

1) The DIP method with the 12-block horizontal enlargement correction reduced the variance of the pixel value of the subtraction image between FIP and BIP images than that of the conventional DIP method.
2) Extension of the image processing time by addition of the 12-block horizontal enlargement correction was less than 10 s.
3) The present study indicates that the DIP method with the 12-block horizontal enlargement correction produces a higher resolutional DIP image compared to the conventional DIP method.

References

1. Kashima I, Sakurai T, Matsuki T, Nakamura K, Aoki H, Ishii M (1994) Intraoral computed radiography using the Fuji computed radiography imaging plate. Oral Surg Oral Med Oral Pathol 78, 239-246.
2. Möystad A, Svanaes DB, Risnes S, Larheim TA, Grondahl HG (1996) Detection of approximal caries with a storage phosphor system. A comparison of enhanced digital images with dental X-ray film. Dentomaxillofac Radiol 25, 202-206.
3. Hildebolt CF, Fletcher G, Yokoyama-Crothers N, Conover G. L, Vannier MW (1997) A comparison of the response of storage phosphor and film radiography to small variations in X-ray exposure. Dentomaxillofac Radiol 26, 147-151.
4. Hintze H, Wenzel A, Frydenberg M (2002) Accuracy of caries detection with four storage phosphor systems and E-speed radiographs. Dentomaxillofac Radiol 31, 170-175.
5. Wenzel A., Møystad A (2010) Work flow with digital intraoral radiography: a systematic review. Acta Odontol Scand 68, 106-114.
6. Kamburoğlu K, Samunahmetoğlu E, Eratam N, Sönmez G, Karahan S (2022) Clinical comparison of intraoral CMOS and PSP detectors in terms of time efficiency, patient comfort, and subjective image quality. Imaging Sci Dent 52, 93-101.
7. Radiopaedia Australia Pty Ltd [Internet]. Photostimulable phosphors; 2005 [Cited 2022 Oct 07] Available from: https://radiopaedia.org/articles/photostimulable-phosphors.
8. Ergün S, Güneri P, Ilgüy D, Ilgüy M, Boyacioglu H (2009) How many times can we use a phosphor plate? A preliminary study. Dentomaxillofac Radiol 38, 42-47.
9. Matsuda Y, Sur J, Araki K, Okano T (2010) Durability of Digora Optime® imaging plates. Oral Radiol 27, 28-34.
10. Souza-Pinto GN, Santaella GM, Coli AA, Oenning AC, Haiter-Neto F (2020) Analysis of the deterioration of photostimulable phosphor plates. Dentomaxillofac

Radiol 49, 20190500.

11. Gulsahi A, Secgin CK (2016) Assessment of intraoral image artifacts related to photostimulable phosphor plates in a dentomaxillofacial radiology department. Niger J Clin Pract 19, 248-253.
12. Çalışkan A, Sumer AP (2017) Definition, classification and retrospective analysis of photostimulable phosphor image artefacts and errors in intraoral dental radiography. Dentomaxillofac Radiol 46, 20160188.
13. American Association of Physicists in Medicine (2006) Acceptance testing and quality control of photostimulable storage phosphor imaging systems, AAPM Report No. 93, 58-60.
14. Watanabe K, Imanishi Y, Kato M, Kimoto H, Sekiguchi T, Amemiya T, Dezawa K, Matsumoto K, Arai Y, Honda K (2022) Preliminary evaluation of dual imaging plate intraoral radiography. J Oral Sci 64, 69-73.
15. Imanishi Y, Sekiguchi T, Kato M, Kimoto H, Amemiya T, Dezawa K, Matsumoto K, Arai Y (2022) Reduction of scratch or dirt artifacts on intraoral radiographs using dual imaging plates in image processing. Oral Radiol. doi: 10.1007/s11282-022-00648-5.
16. White SC, Pharoah MJ (2014) Oral Radiology: Principles and Interpretation. 7th ed, Elsevier Mosby, St Louis, 84-90.
17. Berman HB [Internet] F Distribution Calculator [Cited 2022 Oct 07] Available from: https://stattrek.com/online-calculator/f-distribution.

Tables and Figures

Table 1 Variance of the pixel value in the six sets of subtraction images at each process and *F*-value between each process in the mesh phantom

		F-value				
	Variance	Sub	HV	Rot	EnIH	EnIH12
Sub	1,518.99	-	1.21	3.68	5.21	6.50
HV	1,253.75		-	3.03	4.30	5.37
Rot	413.32			-	1.42	1.77
EnIH	291.65				-	1.25
EnIH12	233.67					-

F critical value: 1.00183 (degree of freedom: 6,479,999, $\alpha = 0.01$). Sub, simple subtraction; HV, correction of horizontal and vertical direction; Rot, correction of rotation; EnlH, correction of enlargement of the horizontal direction; EnlH12, correction of enlargement of the horizontal direction of 12 blocks. Variance of the pixel value in the subtraction images was gradually and significantly decreased by each step of the image processing ($P < 0.01$), indicating that the degree of alignment of the front and back image plates improved during the image processing.

Table 2 Variance of the pixel value in the six sets of subtraction images at each process and *F*-value between each process in the porcine phantom

		F-value				
	Variance	Sub	HV	Rot	EnIH	EnIH12
Sub	129.14	-	1.25	1.48	2.01	2.21
HV	103.25		-	1.18	1.61	1.77
Rot	87.34			-	1.36	1.50
EnIH	64.12				-	1.10
EnIH12	58.36					-

F critical value: 1.00183 (degree of freedom: 6,479,999, $\alpha = 0.01$). Sub, simple subtraction; HV, correction of horizontal and vertical direction; Rot, correction of rotation; EnlH, correction of enlargement of the horizontal direction; EnlH12, correction of enlargement of the horizontal direction of 12 blocks. Variance of the pixel value in the subtraction images was gradually and significantly decreased by each step of the image processing ($P < 0.01$), indicating that the degree of alignment of the front and back image plates for synthesizing DIP images improved during the image processing.

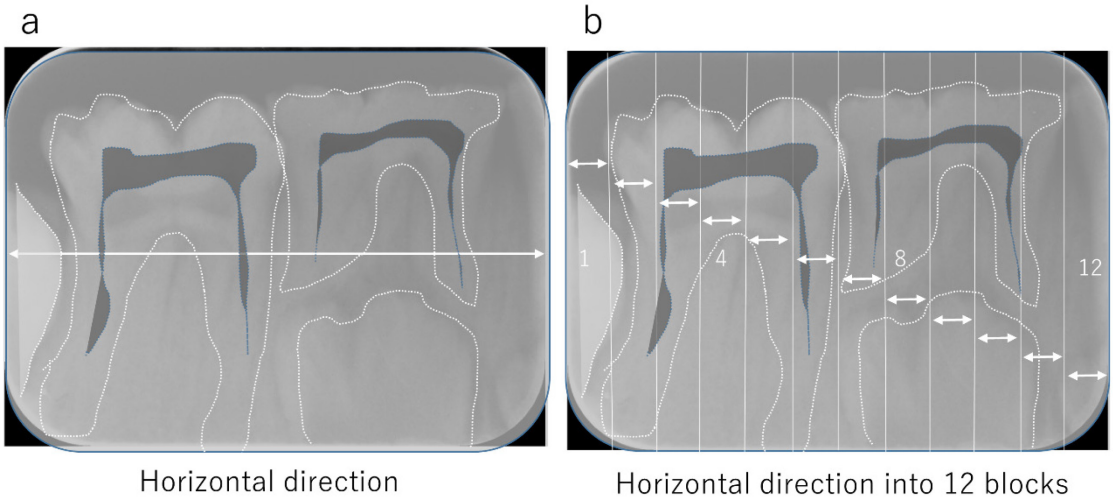

Fig. 1 a: Correction of the horizontal enlargement ratio on the imaging plate (IP). b: The IP was divided into 12 blocks and each enlargement of the ratio was independently corrected.

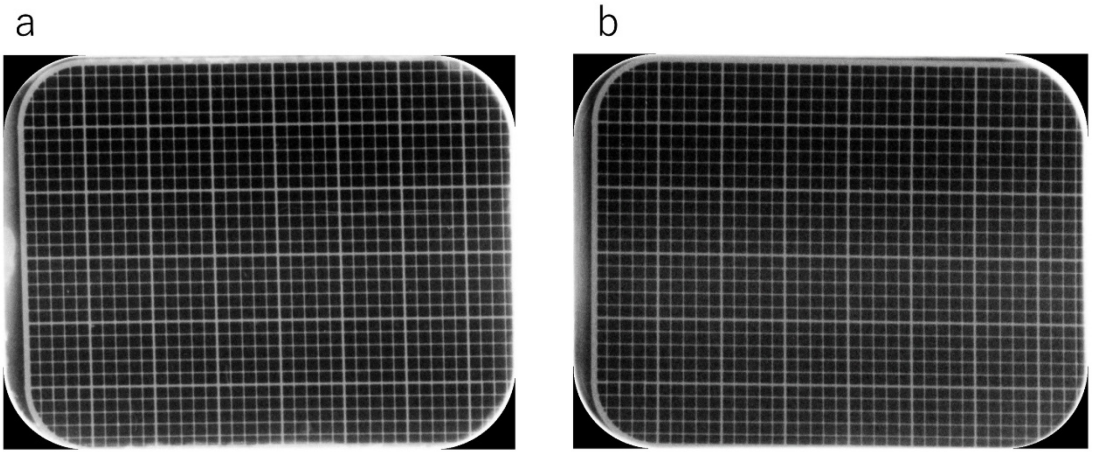

Fig. 2 Sample images of the front imaging plate (a) and back imaging plate (b) of the 1 mm mesh plate phantom.

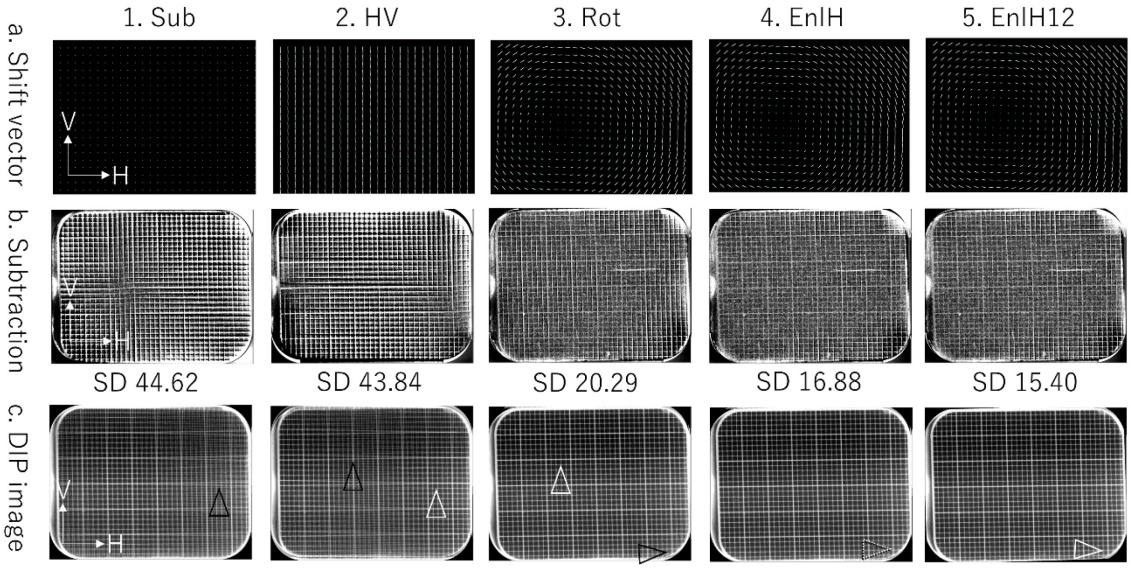

Fig. 3 Steps in dual image processing of the 1mm mesh plate phantom. 1. Sub, simple subtraction; 2. HV, correction of the horizontal and vertical directions; 3. Rot, correction of rotation; 4. EnlH, correction of enlargement of the horizontal direction; 5. EnlH12, correction of enlargement of the horizontal direction of 12 blocks; a, Shift vector showing the shift value of the BIP for each position; b, Subtraction images between FIP and BIP images; c, DIP images.

Double lines or dull edges indicating misalignment between FIP and BIP images are indicated by a black arrowhead on 1c. The alignment improved on 2c (white arrowhead). However, 2c shows double lines indicated by a black arrowhead. The dotted arrowhead on 4c indicates a part that is still slightly misaligned. The dull edge appears smaller on the white circles of 5b and 5c.

DIP, dual imaging plate; FIP, front imaging plate; BIP, back imaging plate; SD, standard deviation: V, vertical direction; H, horizontal direction.

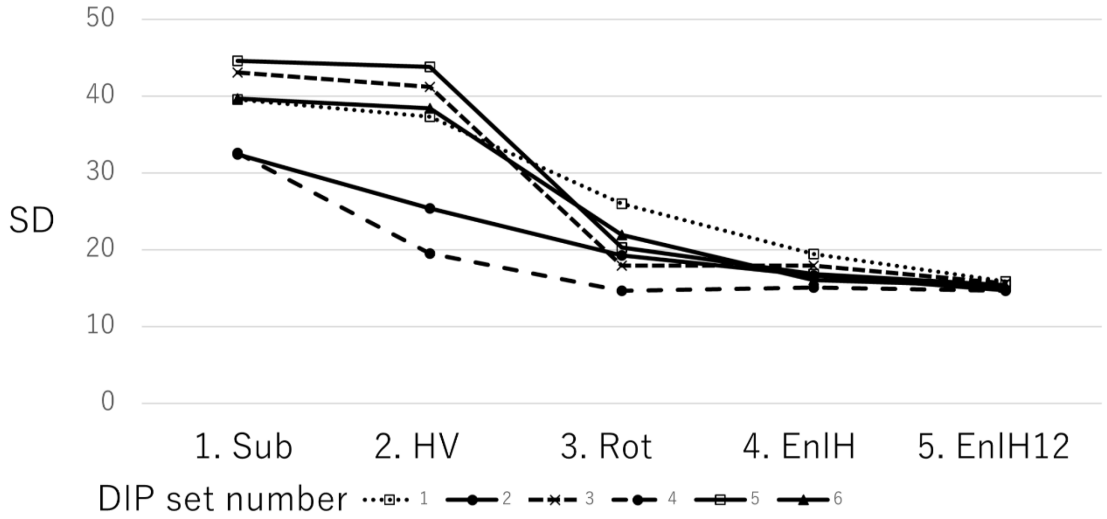

Fig. 4 Correction and SD of subtraction images at each step. Six sets of SD of subtraction images were reduced by each process. 1. Sub, simple subtraction; 2. HV, correction of the horizontal and vertical directions; 3. Rot, correction of rotation; 4. EnlH, correction of enlargement o-f the horizontal direction; 5. EnlH12, correction of enlargement of the horizontal direction of 12 blocks; SD, standard deviation; DIP, dual imaging plate.

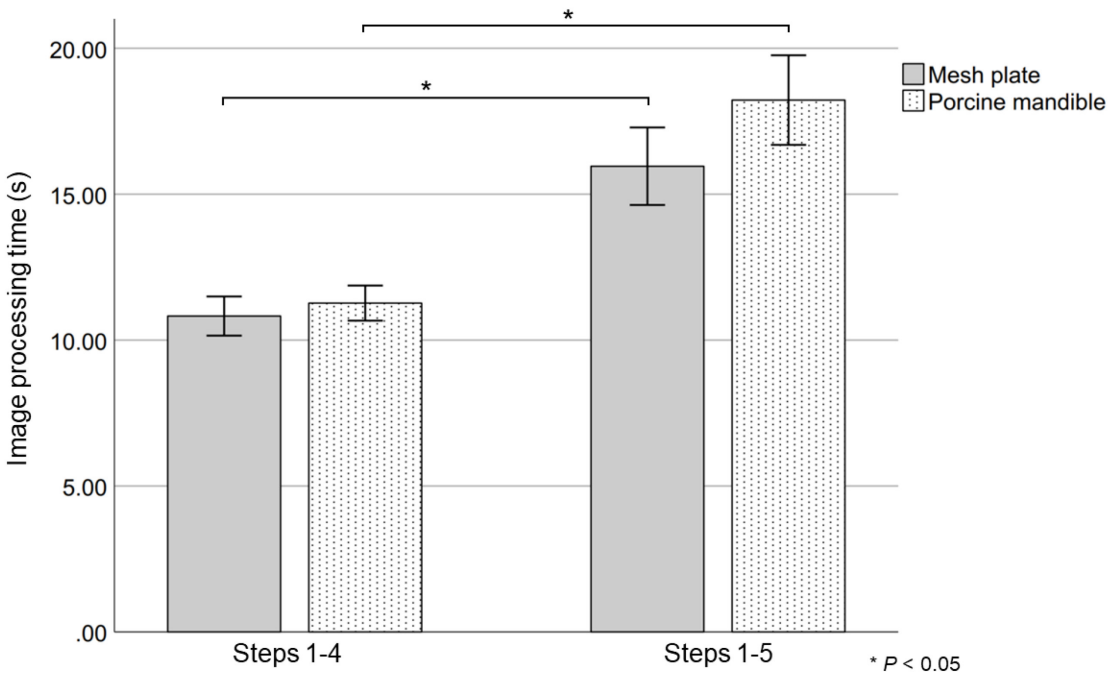

Fig. 5 Image processing time for steps 1–4 and steps 1–5. Statistically significant extensions of the imaging processing time by correcting the enlargement of the horizontal direction by dividing the IP area into 12 blocks can be seen in both the mesh plate and porcine mandible phantoms ($P < 0.05$).

Steps 1–4 include simple subtraction and correction of the horizontal and vertical directions, and rotation and enlargement of the horizontal direction. Steps 1–5 include steps 1–4 together with correction of the enlargement of the horizontal direction by dividing the IP area into 12 blocks. Error bars represent 95% confidence interval.

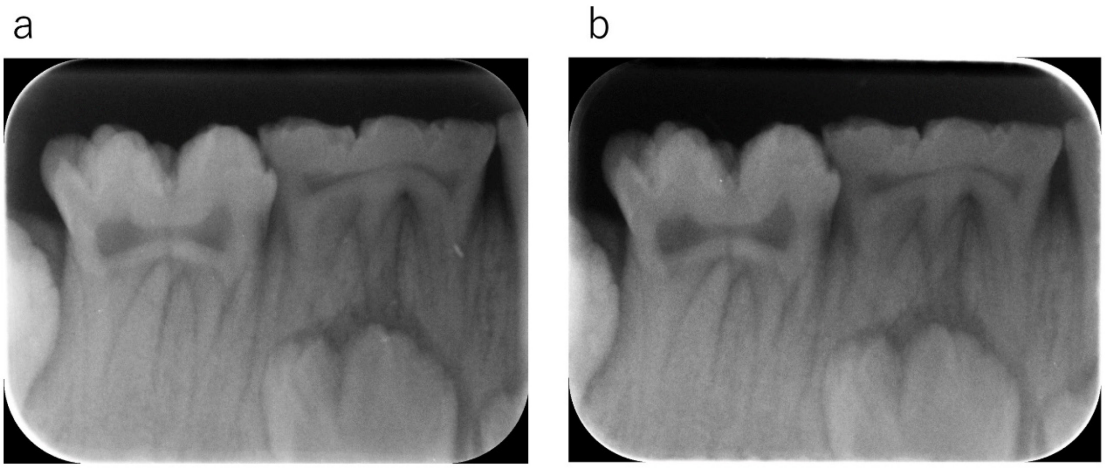

Fig. 6 Sample images of the front imaging plate (a) and back imaging plate (b) of the porcine mandible phantom.

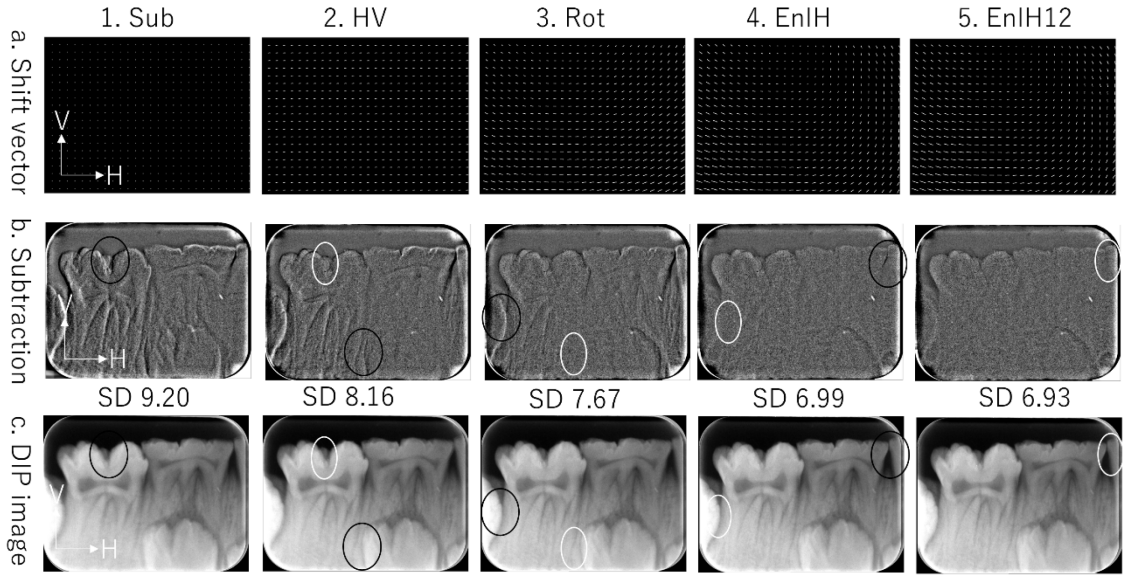

Fig. 7 Steps for processing of the DIP of the porcine mandible phantom. 1. Sub, simple subtraction; 2. HV, correction of the horizontal and vertical directions, 3. Rot, correction of rotation; 4. EnlH, correction of enlargement of the horizontal direction; 5. EnlH12, correction of enlargement of the horizontal direction of 12 blocks; a, Shift vector showing the shift value of the BIP for each position; b, Subtraction images between FIP and BIP images; c, DIP images. Black circles indicate double lines and dull edges. White circles indicate improved and sharper images after each step. DIP, dual imaging plate; FIP, front imaging plate; BIP, back imaging plate; SD, standard deviation; V, vertical direction; H, horizontal direction.